



Contents lists available at ScienceDirect

Physics Letters A

www.elsevier.com/locate/pla

Multifrequency and edge breathers in the discrete sine-Gordon system via subharmonic driving: Theory, computation and experiment

F. Palmero^{a,b}, J. Han^b, L.Q. English^{b,*}, T.J. Alexander^c, P.G. Kevrekidis^{d,e}^a Grupo de Física No Lineal, Departamento de Física Aplicada I, ETSI Informática, Universidad de Sevilla, Avda. Reina Mercedes, s/n, 41012 Sevilla, Spain^b Department of Physics and Astronomy, Dickinson College, Carlisle, PA 17013, USA^c School of Physical, Environmental and Mathematical Sciences, UNSW Canberra, 2610, Australia^d Department of Mathematics and Statistics, University of Massachusetts, Amherst, MA 01003-4515, USA^e Center for Nonlinear Studies and Theoretical Division, Los Alamos National Laboratory, Los Alamos, NM 87544, USA

ARTICLE INFO

Article history:

Received 26 August 2015

Received in revised form 30 October 2015

Accepted 31 October 2015

Available online xxxx

Communicated by C.R. Doering

Keywords:

Intrinsic localized modes

Discrete breathers

Edge breathers

ABSTRACT

We consider a chain of torsionally-coupled, planar pendula shaken horizontally by an external sinusoidal driver. It has been known that in such a system, theoretically modeled by the discrete sine-Gordon equation, intrinsic localized modes, also known as discrete breathers, can exist. Recently, the existence of multifrequency breathers via subharmonic driving has been theoretically proposed and numerically illustrated by Xu et al. (2014) [21]. In this paper, we verify this prediction experimentally. Comparison of the experimental results to numerical simulations with realistic system parameters (including a Floquet stability analysis), and wherever possible to analytical results (e.g. for the subharmonic response of the single driven-damped pendulum), yields good agreement. Finally, we report the period-1 and multifrequency edge breathers which are localized at the open boundaries of the chain, for which we have again found good agreement between experiments and numerical computations.

© 2015 Elsevier B.V. All rights reserved.

1. Introduction

Discrete breathers, also known as intrinsic localized modes, appear widely in damped-driven oscillator systems [1,2], and general conditions for their appearance have been recently established theoretically [3]. Such time-periodic and exponentially localized in space coherent structures have been observed experimentally in a diverse range of nonlinear oscillator systems, including Josephson junction arrays [4,5], coupled antiferromagnetic layers [6], halide-bridged transition metal complexes [7], micro-mechanical cantilever arrays [8,9], electrical transmission lines [10] and torsionally-coupled pendula [11] among others [12–14]. They have also been argued to be of relevance to various biological problems including dynamical models of the DNA double strand [15], as well as more recently in protein loop propagation [16]. Many of the features of the discrete breather response are generic across these wide-ranging experimental systems; see e.g. [17]. However, the intrinsic properties of a single oscillator (as well as, often times, the specific nature of the coupling) may play a key role in the observed dynamics and the nature of the discrete breathers formed in the different physical systems.

Inspired by this observation, recent work has revealed that subharmonic resonances of a single oscillator (see e.g. [18]) may be used to excite discrete breather formation in an electrical lattice [19]. More recently, this idea has been examined further in the context of a horizontally shaken pendulum (which has long been known to display a variety of subharmonic resonances [20]), and the possibility of mixed-frequency breathers was identified in a pendulum chain [21]. These breathers exhibit the remarkable response that while energy is localized on a few pendula responding at a sub-harmonic of the driving force, the pendula in the tails of the breather are oscillating with the driving frequency. To the best of our knowledge, these theoretically proposed and numerically identified subharmonic breathers in the pendulum chain have not yet been experimentally observed. This is one of the key goals of the present work. More specifically, we further investigate these mixed frequency breathers theoretically, and compute them numerically, exploring their spectral and dynamical stability, identifying suitable frequency intervals where they may be expected to persist. We then go on to verify their existence by means of direct experimental observations in a horizontally shaken chain of torsionally-coupled pendula [22,11,23].

We also examine the role of breather location in the dynamics and reveal that discrete breathers may be localized at the end of the pendulum chain. To the best of our knowledge this is the first time the existence of such mechanical oscillator breather

* Corresponding author.

E-mail address: englishl@dickinson.edu (L.Q. English).

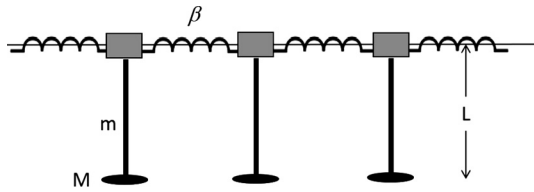


Fig. 1. A schematic of the experimental pendulum chain.

edge states has been experimentally demonstrated. Nevertheless, it should be noted that research interest in edge states has a long history in other fields (see e.g. [25] and references therein), including manifestations in the form of electronic surface waves at the edge of periodic crystals (Tamm states [25]), optical surface modes in waveguide arrays [26], and more recently surface breather solitons in graphene nanoribbons [27].

Our presentation of the relevant results below is structured as follows. In Section 2, we present our theoretical model and discuss its physical parameters (of relevance to the experiment) for a horizontally shaken pendulum chain. The relevant dynamical equation in the form of a damped-driven discrete sine-Gordon system is closely related to the driven-damped form of the famous Frenkel-Kontorova model [24,28]. In Section 3, after theoretically, numerically and experimentally corroborating the subharmonic response of a single pendulum, we seek subharmonic solutions numerically and trace their parametric interval of stability. We are then able to show their existence experimentally, both in the case of “bulk” subharmonic breathers, as well as in the form of edge modes. Finally, in Section 4, we summarize our findings and present some possible directions for future study.

2. The model and experimental setup

The experimental setup is very similar to the one described in detail in Ref. [23] and schematically shown in Fig. 1. Each pendulum experiences four distinct torques – gravitational, torsional, frictional and driving torque. The driving torque arises due to the horizontal shaking of the pendulum array by a high-torque electric motor. The amplitude, A , of the sinusoidal driving was fixed in the experiment, but the frequency, $f = \omega_d/(2\pi)$, was finely tunable (in 0.05 Hz increments) and measured by magnetic sensing. Angles were measured using a horizontal laser beam from a diode laser attached to the frame of the pendulum array; this beam is then periodically interrupted by the swinging pendulum when properly aligned. This method gives an estimated precision of about ± 1 deg. An overhead web-cam was also used to monitor and record the pendulum motion. As a result of the above contributions, the motion of a single (uncoupled) pendulum is well described by the equation,

$$\ddot{\theta} + \left(\frac{\gamma_1}{I}\right)\dot{\theta} + \omega_0^2 \sin \theta + F\omega_d^2 \cos(\omega_d t) \cos \theta = 0, \quad (1)$$

where I is the pendulum’s moment of inertia, $I = ML^2 + \frac{1}{3}mL^2$, the driving strength is given by $F = A\omega_0^2/g$, and ω_0 is the pendulum’s natural frequency of oscillation with $\omega_0^2 = \frac{1}{I}(mgL/2 + MgL)$. Experimentally, the number of pendula is $N = 19$, $L = 25.4$ cm, $m = 13$ g, $M = 14$ g, $\gamma_1 = 500$ gcm²/s, and $A = 0.6$ cm. Pendula at the two ends can oscillate freely (free boundary conditions).

If we add the torsional coupling to nearest-neighbor pendula, i.e., in the presence of all four of the above contributions, Eq. (1) becomes a system of differential equations given by,

$$\ddot{\theta}_n + \omega_0^2 \sin \theta_n - \left(\frac{\beta}{I}\right) \Delta_2 \theta_n + \left(\frac{\gamma_1}{I}\right) \dot{\theta}_n - \frac{\gamma_2}{I} \Delta_2 \dot{\theta}_n + F\omega_d^2 \cos(\omega_d t) \cos \theta_n = 0, \quad (2)$$

where β is the torsional spring constant, and Δ_2 represents the discrete Laplacian. We include an intersite friction term (prefactor γ_2) originating from the energy dissipation due to the twisting of the springs [11]. Here, we assume that nonlinearity in the un-driven array enters only through the sine-function in the gravitational term, but not through the coupling springs. This assumption seems to be experimentally justified for angle differences of up to 90 deg, but it may not work well beyond that. Experimental values of coefficients are $\beta = 0.0083$ Nm/rad and $\gamma_2 = 70$ gcm²/s. These equations can be non-dimensionalized by introducing the following parameters $\omega = \omega_d/\omega_0$, $C = \beta/I\omega_0^2$, $\alpha_1 = \gamma_1/I\omega_0$, $\alpha_2 = \gamma_2/I\omega_0$ and rescaling time $t \rightarrow t/\omega_0$, leading to the following dimensionless equation for the n th pendulum:

$$\ddot{\theta}_n + \sin \theta_n - C \Delta_2 \theta_n + \alpha_1 \dot{\theta}_n - \alpha_2 \Delta_2 \dot{\theta}_n + F\omega^2 \cos(\omega t) \cos \theta_n = 0. \quad (3)$$

For our experimental conditions the dimensionless parameters are $C = 0.16$, $\alpha_1 = 64 \times 10^{-4}$, $\alpha_2 = 9 \times 10^{-4}$ and $F = 0.026$. We use these parameters throughout the theoretical investigations of this work, and consider only variations in the dimensionless frequency parameter ω , which is tunable as indicated above. In our plots we transform back to physical units, plotting results versus driving frequency in Hertz, f , where, for reference, the natural frequency of our pendulum is $f_0 = \omega_0/(2\pi) = 1.04$ Hz.

As numerical simulations have shown that a one-peak breather is mainly localized on a single pendulum and its first neighbors, experimentally, the method used to initiate multifrequency breathers is by manually displacing a group of three pendula through angles roughly predicted by the simulations. Upon release, a true breather mode can then sometimes establish itself, depending on whether the phase of release happened to be sufficiently close in relation to the driver. In practice, it may take a number of such trials before the driver can lock onto the initialized pendula in this manner.

3. Results

We first examine a single damped-driven pendulum. In general, we have observed similar behavior to that found in [21], where the same system was studied in a slightly different range of parameters. Examining the response of the system to different frequencies and amplitudes of the driving force, we obtain the resonance curves shown in Fig. 2. Since a pendulum is an oscillator characterized by soft nonlinearity, we have found experimentally and numerically that the resonance curve exhibits the characteristic bend toward lower frequencies, as is theoretically expected [18]. At higher frequencies we find the well known pendulum subharmonic response [29]. A subharmonic branch starting at around three times the natural frequency can be obtained both in the experiment and in the numerics. Here, the pendulum responds to the driver by swinging at a frequency that is one-third of the driving frequency, f . In this way, for every three periods of the shaken table, the pendulum performs one complete swing. It is also interesting to note that larger response amplitudes can be achieved via subharmonic driving than with direct driving. Numerically we have found higher-order resonances, but these resonances correspond to frequencies not accessible in our experimental setup. In particular, we have found numerical solutions starting at around five and seven times the external driver frequency. Numerical simulations have shown that subharmonic breathers corresponding to these high frequencies are mostly unstable, with the exception of frequencies within very narrow intervals close to the starting frequency value.

In order to get approximate analytical solutions to Eq. (1), we Taylor-expand the trigonometric functions and obtain (in dimensionless form),

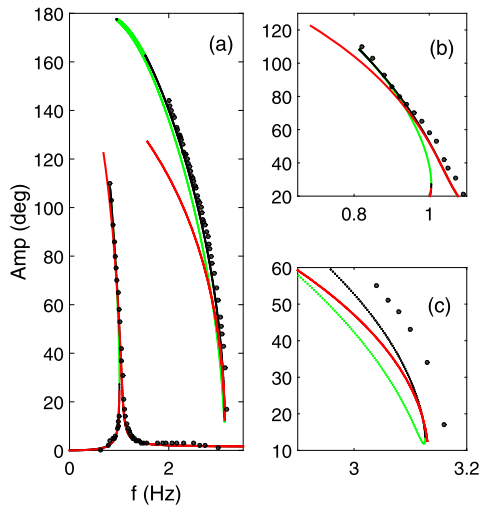


Fig. 2. (Color online.) (a) The response curve of a single driven-damped pendulum. The filled circles indicate experimental data, the black and green lines are numerical results and the red line represents the analytical prediction. Black lines correspond to stable solutions and green to unstable solutions. For the main resonance at around 1 Hz, all three traces agree quite well. Notice, however, that due to the sine-expansion approximation, for the subharmonic resonance, the analytical prediction deviates from the numerical/experimental data for large amplitudes, as expected. (b) Zoom showing the peak corresponding to main resonance. (c) Zoom showing the origin of the subharmonic resonance.

$$\ddot{\theta} + \theta + \left[\alpha_1 \dot{\theta} - \frac{\theta^3}{6} + F\omega^2 \cos(\omega t) \left(1 - \frac{\theta^2}{2} \right) \right] = 0. \quad (4)$$

Assuming that in the main resonance case the solution takes the form,

$$\theta = V \cos(\omega t + \phi), \quad (5)$$

and in the subharmonic case,

$$\theta = V_{1/3} \cos(\omega t + \phi) + V_{1/3} \cos(\omega t + \phi_{1/3}) + A_{1/3} \cos(\omega t/3) + B_{1/3} \sin(\omega t/3), \quad (6)$$

and using the harmonic balance method [30], a set of algebraic equations can be deduced in order to get the values of parameters V , ϕ , $V_{1/3}$, $\phi_{1/3}$, $A_{1/3}$ and $B_{1/3}$. Approximate resonance curves have been obtained, as shown in Fig. 2. We note that these approximate solutions show good agreement in the main resonance case (as previously also indicated in Ref. [21]), but also in the subharmonic resonance case when the amplitude oscillations are not too large. It is relevant to point out here that the Taylor expansion utilized in order to obtain the analytical results is only valid for small values of θ ; in that light, the range of agreement of the theoretical results with the experimental (and numerical) ones is well beyond the realm of applicability of the theoretical approximation.

Having mapped out the response regime for a single pendulum, let us now turn to the full pendulum array. The existence of period-1 breather solutions has already been established experimentally for this system [23]. As a check, we start with the known period-1 breather and verify that experiments and numerics are in good agreement. This is demonstrated in Fig. 3 which depicts the maximum amplitude of oscillation for each pendulum. Numerical simulations performed with longer chains ($N = 41$) show that this behavior is independent of the length of the chain. Note that the small range of frequencies for which the solutions exist is directly related to the region of bistability in the single-pendulum case, as shown in [21].

Let us now consider the pendulum array in the case of the subharmonic response of the chain. One might expect when turning on the coupling and moving away from the anti-continuous limit

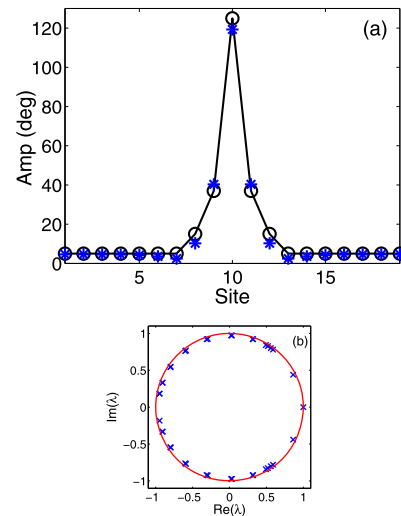


Fig. 3. The pendulum array: (a) The period-1 breather profile depicted as the maximum amplitude of each pendulum (no phase information). Experimental (numerical) angles are indicated by circles (stars). (b) The Floquet multipliers for the breather solution shown in the left panel are all within the unit circle, indicating its spectral stability. Both solutions correspond to a frequency of 0.91 Hz.

that a multifrequency breather would emerge, in which the center pendulum performs periodic (subharmonic) motion, while the pendula in the wings respond weakly at the driving frequency. Previous numerical studies have shown that, for a different range of control parameter values, and close to the subharmonic bifurcation ($f \approx 3$ Hz), this breather exists but is unstable, except for small frequency windows below the bifurcation point [21]. In our system, in contrast, we have been able to identify such a mode experimentally for a range of frequencies, and its existence and dynamical stability have been corroborated by numerical computations. It should also be noted that, in general, the precise stability details of such a subharmonic breather depend strongly on the number of pendula in the chain, with a smaller N favoring more robust configurations, as indicated in [21]. Nevertheless, in our case, numerical simulations in longer chains suggest that the breather remains stable.

The mode profile corresponding to a frequency close to 2 Hz is mapped out in Fig. 4(a). The x -axis denotes the node index, and the y -axis plots the angles (away from vertically down) at the instantaneous turning point of the center pendulum. Note the excellent agreement between experiment and simulations in the left panel at around 1.95 Hz. In both traces, the center pendulum oscillates between roughly 180° and -180° . In further agreement with numerical results, the peak of the experimental breather is observed to be out-of-phase with the tails at the turn-around points of the center pendulum (i.e., an out-of-phase breather), as shown in Fig. 5. It should be noted that the angles of only the breather center and neighboring pendulum on one side were experimentally measured to high precision, but that the breathers were visually found to be very close to symmetric about the ILM-center.

Fig. 4(b) shows the Floquet multipliers of this solution demonstrating its stability. Numerical simulations performed with longer chains ($N = 41$) show that this behavior is independent of the length of the chain. Fig. 4(c) shows a snapshot recorded by the overhead camera for a driver frequency of 1.75 Hz. The mode is sharply localized with one pendulum acquiring an amplitude exceeding 180° .

It is illuminating to study, experimentally and numerically, the effect of the driver frequency on the profile of this multifrequency breather. Fig. 6 maps out the amplitude of this breather solution as a function of the frequency; it thus represents a response curve

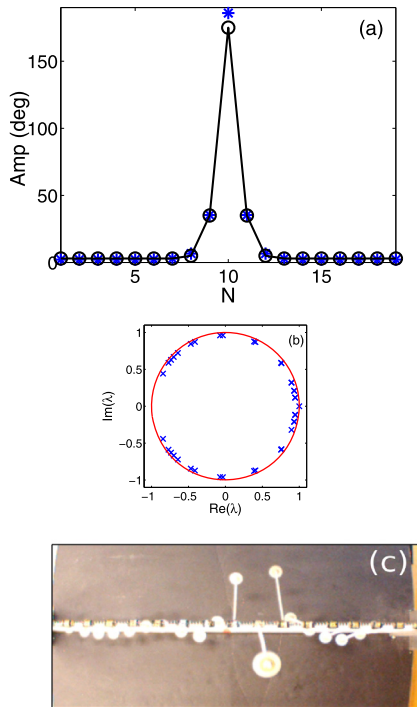


Fig. 4. The pendulum array: (a) The subharmonic breather profile corresponding to 1.95 Hz depicted as the maximum amplitude of each pendulum (no phase information). Experimental (numerical) angles are indicated by circles (stars). (b) The Floquet multipliers for the breather solution shown in (a) are all within the unit circle, indicating breather stability. (c) The pendula as seen by the overhead web-cam. The multibreather mode at 1.75 Hz is sharply localized and the center pendulum is clearly seen to exceed 180 deg.

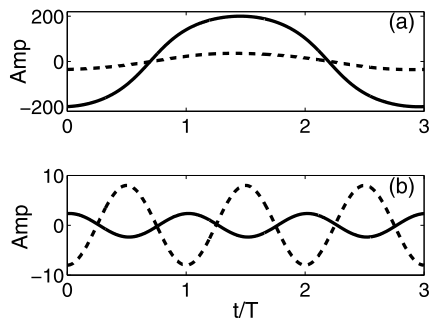


Fig. 5. Numerical mixed-frequency breather trajectory across one period ($T = 2\pi/\omega$) for $f = 1.95$ Hz and $N = 19$ (amplitude in degrees). (a) Trajectory corresponding to central peak pendulum (continuous line) and its first neighbor (dashed line). (b) Trajectory corresponding to the edge pendulum at the end of the chain (continuous line) and normalized external driving force (dashed line), that is proportional to $-\cos(\omega_d t)$.

for the multifrequency breather. We see that over much of the frequency interval that exhibited a subharmonic response in the single pendulum, the breather solution is unstable against perturbations. There is, however, one band around 2 Hz and another narrow band around 3 Hz in which the multifrequency breather is predicted to be stable. Around 2 Hz, the stable breather is out-of-phase, by which we mean that the center and the tails are out of phase. At 3 Hz, the stable breathers are more spread along the chain and the subharmonic frequency component (originating from the center pendulum) is still somewhat present at the tails.

In our numerical study, where we have considered the frequency as a control parameter, we have identified two different stable subharmonic breather solutions – one at high frequency around 3 Hz and the other at low frequency around 2 Hz. Also note that there are two numerical solutions at each driver frequency

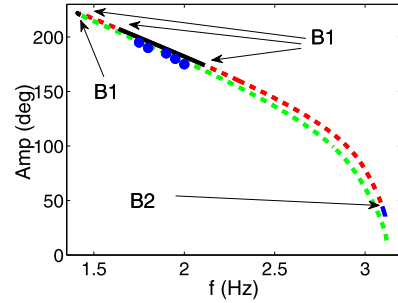


Fig. 6. (Color online.) Amplitude in degrees plotted against the driver frequency corresponding to subharmonic breather families. The continuous black and blue lines indicate the two different regimes of stable numerical breathers (around 2 and 3 Hz, respectively). The dotted red lines show the unstable breathers. The (blue) circles depict the experimental results. Notice the two frequency intervals of stability – one around 2 Hz, and the other, very small, around 3 Hz. The different bifurcations (B1: Bifurcation associated with a conjugate pair of complex Floquet multipliers crossing the unit circle bifurcation; B2: Bifurcation associated with a real Floquet multiplier crossing the unit circle) lead to the destabilization of the breathers. The relevant scenarios are discussed in detail in the text.

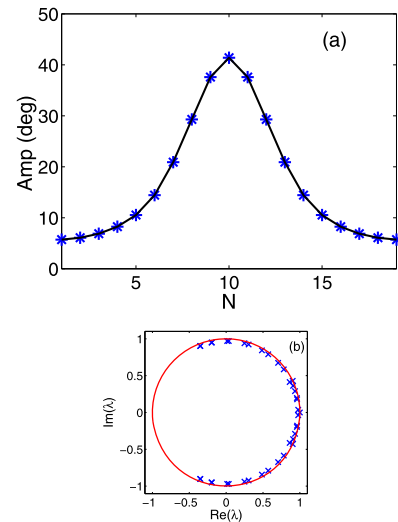


Fig. 7. Stable breather-like solutions corresponding to frequencies close to 3 Hz. (a) Breather profile (maximum amplitude in degrees) and (b) Floquet exponents corresponding to 3.1 Hz (one site breather).

(shown in Fig. 6 as red and green dotted lines), but the smaller-amplitude solution (green line) is always found to be unstable. For the low-frequency family (around 2 Hz), the transition from stability to instability proceeds via a bifurcation associated with a conjugate pair of complex Floquet multipliers crossing the unit circle (B1), a Neimark–Sacker bifurcation (NSB). However, for the high-frequency breather family (around 3 Hz), the relevant destabilization arises through a real multiplier crossing the unit circle at (1, 0), as shown in detail in Fig. 7.

In agreement with our numerical results, in our experiments it has been possible to detect an interval of frequencies around 2 Hz where the subharmonic breather exists. Furthermore, the NSB has been observed in experiments, occurring when a stable subharmonic breather, after a slight variation in the driver frequency, experiences oscillations that grow in amplitude until the breather finally vanishes. This type of instability also occurs for the period-1 breather and was experimentally tracked and illustrated in Ref. [22].

The question then arises if breathers can also be observed within the high-frequency interval (around 3 Hz). We find numerically that indeed stable solutions can be found, but that small variations in the frequency value can drive the system to switch

between two different solutions. These solutions correspond to one site and two site breathers, centered on different points of the lattice, but far from the boundaries. However, a detailed study of these states is beyond the scope of this paper. Simulations in longer chains show essentially the same phenomenon. In experiments, in general, and for long time intervals, one-site and two-site breather-like transient states have been observed.

We now turn to another type of nonlinearly localized mode that can be observed in the pendulum chain system, namely a mode that is localized at the chain boundary. Such modes have been extensively studied in other contexts such as nonlinear optics [31], yet we are not aware of such robust, experimentally demonstrated examples in pendulum arrays. It should also be noted that such modes have also been recently created in other damped-driven mechanical systems such as e.g. granular crystals [32]. As before, the two boundaries are open, and the driving is spatially homogeneous. Nonetheless, we can demonstrate both experimentally and numerically the existence (and stability) of modes localized over a few pendula near the edges of the chain with the interior pendula almost at rest. We find an edge state may be excited independently of the behavior at the other edge. An example with both edges excited is shown in Fig. 8. The driver frequency (as well as the response frequency) here is chosen below the linear dispersion curve at $f = 0.92$ Hz. Note that the linear standing-wave modes are confined to the interval between 1.04 Hz and 1.34 Hz. The experimental data (circles) and the numerical simulation (stars) show close agreement – in both cases, the edge pendula attain an amplitude of oscillation of roughly 100° , whereas the next pendula further in are found to be below 40° in amplitude. Floquet analysis demonstrates that the numerical profile is indeed stable, corroborating the experimental observability of the relevant mode. We find that an edge breather typically has a lower maximum amplitude than the corresponding bulk breather, and it exhibits a more extended domain of stability.

As is evident in the numerical simulations, the amplitude of this edge-breather is frequency dependent, with lower driver frequencies giving rise to larger angles. It is clear that this mode should not be confused with a linear standing wave, where the edges also exhibit large oscillations. For instance, the second mode (just above the uniform mode) corresponding to a frequency of 1.048 Hz has the two pendula at the opposite edges oscillating π out-of-phase. The nonlinear mode discussed here, however, oscillates in-phase and is sharply localized at the edges with interior pendula almost at rest. Furthermore, numerical simulations in longer chains show the same phenomenon.

It is relevant to point out that a subharmonic version of these edge-breathers also exists around a frequency, f , of 3 Hz. Fig. 9 presents the experimental data as black circles ($f = 3.04$ Hz). We see that the edge pendulum swings with an amplitude of around 75° , but crucially now at a third of the driver frequency, $f/3$. The response of the interior pendula, in contrast, is dominated by the driver frequency, f . This mode was found to persist throughout the time horizon of our experiments.

Fig. 9 superimposes two numerical traces for two closely-spaced driver frequencies ($f = 2.97$ Hz and 3.11 Hz). The first one (squares) matches the experimental observation very well, but Floquet analysis reveals it to be weakly unstable. In fact, the instability is of the NS type, in contrast to the previous subharmonic breather (in the chain interior). The second numerical trace (stars) features a slightly larger f , and is stable, but departs from the experimental profile. It is likely that either small lattice inhomogeneities or weak nonlinearities in the torsional springs were responsible for stabilizing the observed multifrequency edge mode in the experiment.

We remark that, in general, wherever an intrinsic localized mode appears there is also the possibility of a stable small am-

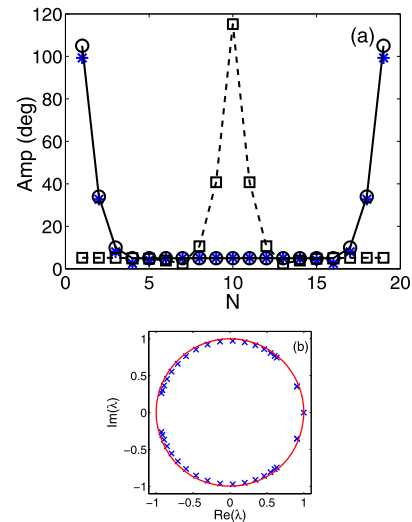


Fig. 8. A nonlinearly localized edge state for $f = 0.92$ Hz: (a) The edge breather profile – experimental (numerical) results are shown as circles (stars). Numerically stable breather located at the chain center and corresponding to the same frequency is shown as squares. (b) The Floquet multipliers for the edge breather are all within the unit circle indicating stability.

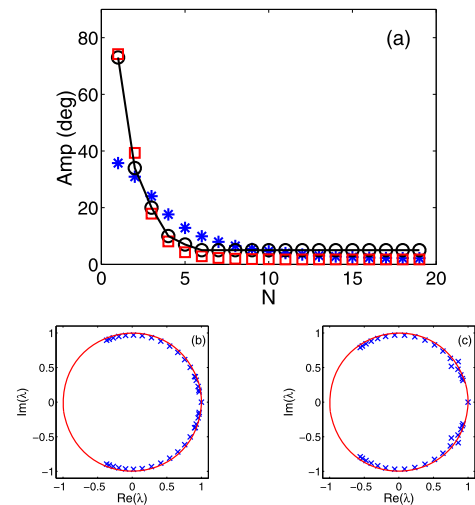


Fig. 9. A multifrequency edge breather driven subharmonically near $f = 3.0$ Hz. (a) The experimental profile found for $f = 3.04$ Hz is depicted as black circles. In addition, two numerical solutions are shown: the red squares represent a solution at $f = 2.97$ Hz that is found to be weakly unstable, see (c). The blue stars depict a nearby solution that is dynamically stable, see (b), corresponding to $f = 3.11$ Hz.

plitude delocalized oscillation. This is because such an oscillation forms the tails of the intrinsic localized mode. It is thus important to have an initial condition which is close to the intrinsic localized mode, otherwise only the low amplitude oscillation will be observed.

4. Conclusions

In the present work, we revisited the chain of coupled torsion pendula, an experimental setup for which there is a well-established theoretical model accounting for torsional contributions from gravity, nearest neighbors, friction and external drive. This damped-driven system was previously found to feature prototypical discrete breather waveforms. Recent explorations [21] have suggested the possibility of subharmonic breather structures, which, in general, were unstable for larger chains but potentially stable for smaller lattices. In the present work, we have con-

firmed the existence of these subharmonic breathers via a combination of theoretical modeling (and where possible analysis), numerical computation, and experimental realization and found that for our parameter choices they are robust even in the long chain case. In addition to uncovering the existence of these subharmonic breathers and their good agreement with experimental observations, we have also revealed period-1 breathers and surface breather modes, which have also been experimentally identified.

Clearly, this system is a prototypical one for the exploration of nonlinear structures, and their properties and interactions. There are multiple directions for future work, including the study of modulational instability (MI) as a source for the generation of the breathers, the study of breather–breather or breather–impurity interactions and scattering, and the examination of multipeak breather structures, among many others. The multipeak structures in particular have emerged as being relevant here due to their apparent connection to the stable breathers existing in the small high-frequency window. A number of these topics are presently under investigation and will be reported in future publications.

Acknowledgements

F.P. acknowledges Dickinson College's hospitality and support. P.G.K. gratefully acknowledges the support of NSF-DMS-1312856, BSF-2010239, as well as from the US-AFOSR under grant FA9550-12-1-0332, and the ERC under FP7, Marie Curie Actions, People, International Research Staff Exchange Scheme (IRSES-605096). The work of PGK at Los Alamos is partially supported by the US Department of Energy.

References

- [1] J.L. Marín, S. Aubry, *Nonlinearity* 9 (1996) 1501.
- [2] S. Aubry, *Physica D* 103 (1997) 201.
- [3] D. Hennig, *AIP Adv.* 3 (2013) 102127.
- [4] E. Trías, J.J. Mazo, T.P. Orlando, *Phys. Rev. Lett.* 84 (2000) 741.
- [5] P. Binder, D. Abrahimov, A.V. Ustinov, S. Flach, Y. Zolotaryuk, *Phys. Rev. Lett.* 84 (2000) 745.
- [6] U.T. Schwarz, L.Q. English, A.J. Sievers, *Phys. Rev. Lett.* 83 (1999) 223.
- [7] B.I. Swanson, J.A. Brozik, S.P. Love, G.F. Strouse, A.P. Shreve, A.R. Bishop, W.-Z. Wang, M.I. Salkola, *Phys. Rev. Lett.* 82 (1999) 3288.
- [8] M. Sato, B.E. Hubbard, A.J. Sievers, B. Ilic, D.A. Czaplewski, H.G. Craighead, *Phys. Rev. Lett.* 90 (2003) 044102.
- [9] M. Sato, B.E. Hubbard, L.Q. English, A.J. Sievers, B. Ilic, D.A. Czaplewski, H.G. Craighead, *Chaos* 13 (2003) 702.
- [10] L.Q. English, R. Basu Thakur, R. Stearrett, *Phys. Rev. E* 77 (2008) 066601; see also F. Palmero, L.Q. English, J. Cuevas, R. Carretero-González, P.G. Kevrekidis, *Phys. Rev. E* 84 (2011) 026605.
- [11] J. Cuevas, L.Q. English, P.G. Kevrekidis, M. Anderson, *Phys. Rev. Lett.* 102 (2009) 224101.
- [12] H.S. Eisenberg, Y. Silberberg, R. Morandotti, A.R. Boyd, J.S. Aitchison, *Phys. Rev. Lett.* 81 (1998) 3383.
- [13] B. Eiermann, Th. Anker, M. Albiez, M. Taglieber, P. Treutlein, K.P. Marzlin, M.K. Oberthaler, *Phys. Rev. Lett.* 92 (2004) 230401.
- [14] N. Boechler, G. Theocharis, S. Job, P.G. Kevrekidis, M.A. Porter, C. Daraio, *Phys. Rev. Lett.* 104 (2010) 244302.
- [15] M. Peyrard, *Nonlinearity* 17 (2004) R1.
- [16] A.K. Sieradzian, A. Niemi, X. Peng, *Phys. Rev. E* 90 (2014) 062717.
- [17] S. Flach, A.V. Gorbach, *Phys. Rep.* 467 (2008) 1.
- [18] A.H. Nayfeh, D.T. Mook, *Nonlinear Oscillations*, John Wiley & Sons, Inc., 1979.
- [19] L.Q. English, F. Palmero, P. Candiani, J. Cuevas, R. Carretero-González, P.G. Kevrekidis, A.J. Sievers, *Phys. Rev. Lett.* 108 (2012) 084101.
- [20] R.A. Struble, J.A. Marlin, Q. J. Mech. Appl. Math. 18 (1965) 405.
- [21] Y. Xu, T.J. Alexander, H. Sidhu, P.G. Kevrekidis, *Phys. Rev. E* 90 (2014) 042921.
- [22] R. Basu Thakur, L.Q. English, A.J. Sievers, *J. Phys. D* 41 (2008) 015503.
- [23] L.Q. English, Experimental results in pendula arrays, in: J. Cuevas, et al. (Eds.), *The Sine-Gordon Model and Its Applications*, Springer, 2014.
- [24] O.M. Braun, Yu.S. Kivshar, *Phys. Rep.* 306 (1998) 1.
- [25] S.G. Davidson, M. Steslicka, *Basic Theory of Surface States*, Oxford Science, New York, 1996.
- [26] I.L. Garanovich, A.A. Sukhorukov, Yu.S. Kivshar, *Phys. Rev. Lett.* 100 (2008) 203904.
- [27] A.V. Savin, Yu.S. Kivshar, *Phys. Rev. B* 81 (2010) 165418.
- [28] J. Cuevas, P.G. Kevrekidis, F.L. Williams (Eds.), *The Sine-Gordon Model and Its Applications: From Pendula and Josephson Junctions to Gravity and High Energy Physics*, Springer-Verlag, Heidelberg, 2014.
- [29] W. Chester, *IMA J. Appl. Math.* 15 (1975) 289.
- [30] A.A. Qaisia, M.N. Hamdan, *J. Sound Vib.* 305 (2007) 772.
- [31] S. Suntsov, K.G. Makris, D.N. Christodoulides, G.I. Stegeman, A. Haché, R. Morandotti, H. Yang, G. Salamo, M. Sorel, *Phys. Rev. Lett.* 96 (2006) 063901; C.R. Rosberg, D.N. Neshev, W. Krolikowski, A. Mitchell, R.A. Vicencio, M.I. Molina, Yu.S. Kivshar, *Phys. Rev. Lett.* 97 (2006) 083901; B. Alfassi, C. Rotschild, O. Manela, M. Segev, D.N. Christodoulides, *Phys. Rev. Lett.* 98 (2007) 213901; A. Szameit, Y.V. Kartashov, F. Dreisow, T. Pertsch, S. Nolte, A. Tünnermann, L. Torner, *Phys. Rev. Lett.* 98 (2007) 173903; X. Wang, A. Bezryadina, Z. Chen, K.G. Makris, D.N. Christodoulides, G.I. Stegeman, *Phys. Rev. Lett.* 98 (2007) 123903.
- [32] C. Hoogeboom, Y. Man, N. Boechler, G. Theocharis, I.G. Kevrekidis, C. Daraio, *Europhys. Lett.* 101 (2013) 44003.